

PDDFormer: Pairwise Distance Distribution Graph Transformer for Crystal Material Property Prediction

Xiangxiang Shen¹, Zheng Wan¹, Lingfeng Wen¹, Licheng Sun¹, Ou Yang Ming Jie¹, JiJun Cheng¹, XUAN TANG¹, Xian Wei^{1*}

¹East China Normal University
xian.wei@tum.de

Abstract

The crystal structure can be simplified as a periodic point set repeating across the entire three-dimensional space along an underlying lattice. Traditionally, methods for representing crystals rely on descriptors like lattice parameters, symmetry, and space groups to characterize the structure. However, in reality, atoms in material always vibrate above absolute zero, causing continuous fluctuations in their positions. This dynamic behavior disrupts the underlying periodicity of the lattice, making crystal graphs based on static lattice parameters and conventional descriptors discontinuous under even slight perturbations. To this end, chemists proposed the Pairwise Distance Distribution (PDD) method, which has been used to distinguish all periodic structures in the world’s largest real materials collection, the Cambridge Structural Database. However, achieving the completeness of PDD requires defining a large number of neighboring atoms, resulting in high computational costs. Moreover, it does not account for atomic information, making it challenging to directly apply PDD to crystal material property prediction tasks. To address these challenges, we propose the atom-Weighted Pairwise Distance Distribution (WPDD) and Unit cell Pairwise Distance Distribution (UPDD) for the first time, incorporating them into the construction of multi-edge crystal graphs. Based on this, we further developed WPDDFormer and UPDDFormer, graph transformer architecture constructed using WPDD and UPDD crystal graphs. We demonstrate that this method maintains the continuity and completeness of crystal graphs even under slight perturbations in atomic positions. Moreover, by modeling PDD as global information and integrating it into matrix-based message passing, we significantly reduced computational costs. Comprehensive evaluation results show that WPDDFormer achieves state-of-the-art predictive accuracy across tasks on benchmark datasets such as the Materials Project

and JARVIS-DFT.

1 Introduction

Crystals are solids with a regular geometric shape formed by atoms, ions, or molecules arranged periodically in space during the crystallization process. Their structure is typically described using repeating unit cells and lattice vectors. However, this method of description brings a fundamental challenge: the same crystal structure can be represented by different unit cells and lattice vectors, as shown in Figure 1. Additionally, in real-world scenarios, the experimental coordinates of unit cells and atoms are inevitably affected by atomic vibrations and measurement noise. These subtle disturbances can lead to discontinuous changes in any simplified unit cell [Kurlin, 2024], resulting in numerous different unit cells for a given crystal structure, as shown in Figure 1, thereby introducing ambiguity in the representation of crystal data [Widdowson and Kurlin, 2022]. Currently, many graph neural networks [Batzner *et al.*, 2022; Yan *et al.*, 2022; Yan *et al.*, 2024a; Yan *et al.*, 2024b] typically use unit cell parameters, simplified cell parameters, symmetry, and space groups to represent the periodic structure of crystals. However, these features are either non-invariant or discontinuous [Zwart *et al.*, 2008] invariants, leaving the issue of ambiguity in crystal data unresolved [Patterson, 1944; Widdowson *et al.*, 2022; Groom *et al.*, 2016; Bartók *et al.*, 2013; Wassermann *et al.*, 2010; Ahmad *et al.*, 2018].

The continuous and complete invariant—Pairwise Distance Distribution (PDD)—proposed by Widdowson and Kurlin (2022) addresses the ambiguity in crystal data representation by distinguishing all periodic structures in the world’s largest real material collection, the Cambridge Structural Database. To achieve completeness, PDD requires a predetermined number of sufficient neighbors, which is computationally expensive and difficult to directly apply for predicting crystal properties [Balasingham *et al.*, 2022]. [Balasingham *et al.*, 2024] employed distance distribution graphs (DDGs) based on PDD to predict the properties of crystal materials, but they did not achieve satisfactory performance (only slightly better than CGCNN), and although this approach reduced computational costs, it compromised the completeness of PDD. In contrast, crystal graph representations based on multi-edge crystal graphs and unit cell param-

*Corresponding author

eters [Taniai *et al.*, 2024; Yan *et al.*, 2024a] achieve completeness, more accurately characterizing crystal structures and achieving state-of-the-art performance in crystal material property prediction tasks. However, the use of unit cell parameters leads to discontinuities in the crystal graphs.

Since PDD does not account for atomic types, it is challenging to use it directly for effective crystal property prediction. To better represent crystal structures, we first introduce atom-Weighted PDD (WPDD) and intra-Unit cell PDD (UPDD). Furthermore, we integrate WPDD and UPDD into the construction of multi-edge crystal graphs and propose the PDD Graph Transformer (including WPDDFormer and UPDDFormer) based on the transformer architecture. We model WPDD as global information and incorporate it into matrix-based message passing, significantly reducing computational costs (as shown in Table 3). Finally, we employ the Earth Mover’s Distance (EMD) [Rubner *et al.*, 2000] to assess the continuity of crystal graphs, demonstrating that WPDD crystal graphs constructed using only Euclidean distances maintain continuity and completeness under slight atomic position perturbations, providing a more accurate depiction of real crystal structures. Ablation experiments show the crucial role of (W/U)PDD in constructing crystal graphs. Through comprehensive evaluations, our method achieves state-of-the-art predictive accuracy across various tasks in the Materials Project [Chen *et al.*, 2019] and JARVIS-DFT [Choudhary *et al.*, 2020] datasets. This advancement highlights the effectiveness of WPDDFormer in bridging the gap between traditional crystal descriptors and dynamic atomic behavior, leading to more accurate and reliable predictions in materials science.

2 Preliminaries

In this section, we introduce the definitions of crystal structures, PDD, isometric crystal graphs, and the continuity and geometric completeness of crystal graphs. Additionally, we provide in Appendix B the definition and proof of the unique geometric constraints of crystals.

2.1 The structure of crystals

By selecting an appropriate structural unit, the entire crystal structure can be viewed as the periodic repetition of this unit in space. This property, where atoms within a crystal repeat in three-dimensional space according to a specific pattern, is called periodicity, with the smallest repeatable structural unit being the unit cell. The unit cell can be defined as $\mathcal{U} = (\mathcal{X}, \mathcal{P})$, where \mathcal{X} and \mathcal{Z} can be represented in matrix form. Typically, $\mathcal{X} = [x_1, x_2 \cdots x_{n-1}, x_n]^T \in \mathbb{R}^{n \times 1}$, where n represents the number of atoms and $x_i \in \mathbb{R}^1$ represents the atomic type of atom i in the unit cell. $\mathcal{P} = [p_1, p_2 \cdots p_{n-1}, p_n]^T \in \mathbb{R}^{n \times 3}$ is the atomic position matrix, where $p_i \in \mathbb{R}^3$ represents the Cartesian coordinates of the atom i in the unit cell in 3D space. The lattice vectors $\mathcal{L} = [l_1, l_2, l_3]^T \in \mathbb{R}^{3 \times 3}$ can reflect the way the unit cell repeats in three directions to map the periodic crystal structure. Therefore, in 3D space, the infinite crystal structure \mathcal{S} can be represented as $(\mathcal{U}, \mathcal{L})$.

2.2 Continuity and geometric completeness of crystal graphs

Definition 1: Pointwise Distance Distribution. For the infinite crystal structure $\mathcal{S} = (\mathcal{U}, \mathcal{L})$ mentioned in Section 2.1, fix a neighbor count $k \geq 1$. For each point x_i in the unit cell \mathcal{U} , let $d_{i1} \leq \cdots \leq d_{ik}$ be the Euclidean distances from \mathbf{p}_i to its k nearest neighbors in the infinite crystal structure. Consider an $n \times k$ matrix composed of n rows of distance vectors, where each point $x_i \in \mathcal{U}$ corresponds to one row. If the matrix contains $m \geq 1$ identical rows, they are merged into one row with a weight of $\frac{m}{n}$. The resulting matrix can be regarded as a weighted distribution of rows, which is called the Pointwise Distance Distribution $\mathcal{PDD}(\mathcal{S}; k) \in \mathbb{R}^{n \times (k+1)}$.

Definition 2: Isometric Crystal Graphs. According to the definition from [Widdowson and Kurlin, 2022] and [Yan *et al.*, 2024a], an isometric transformation is a mapping that preserves Euclidean distances, denoted as $f(x) = Rx + b$. Any isometric transformation f can be decomposed into translation, rotation, and reflection. Specifically, suppose there exists a rotation matrix $R \in \mathbb{R}^{3 \times 3}$, with a determinant of 1 ($|R| = 1$), and a translation vector $b \in \mathbb{R}^3$, then two crystal structures $\mathcal{S} = (\mathcal{U}, \mathcal{L})$ and $\mathcal{Q} = (\mathcal{U}', \mathcal{L}')$ are isometric, satisfying $\mathcal{U}' = R\mathcal{U} + b$, where $R\mathcal{U} + b$ denotes the application of the rotation R and translation b to each element in the infinite set \mathcal{U} .

If \mathcal{S} and \mathcal{Q} are isometric, then their crystal graph representations satisfy $\mathcal{G}(\mathcal{S}) = \mathcal{G}(\mathcal{Q})$, which means that the graphical representation of the crystal structure produces no false positives; that is, there are no isometric pairs where $\mathcal{G}(\mathcal{S}) \neq \mathcal{G}(\mathcal{Q})$ but $\mathcal{S} \simeq \mathcal{Q}$. Conversely, if $\mathcal{G}(\mathcal{S}) = \mathcal{G}(\mathcal{Q})$, then \mathcal{S} and \mathcal{Q} are isometric, meaning f produces no false negatives, i.e., there are no non-isometric pairs where $\mathcal{G}(\mathcal{S}) = \mathcal{G}(\mathcal{Q})$ but $\mathcal{S} \not\simeq \mathcal{Q}$. That is, if the crystal graph representations of artificially constructed crystal structures are identical under isometric transformations, then they are geometrically equivalent.

Definition 3: Geometrically Complete Crystal Graphs. According to [Widdowson and Kurlin, 2022] and [Yan *et al.*, 2024a], if we construct crystal graphs $\mathcal{G}(\mathcal{S}) = \mathcal{G}(\mathcal{Q}) \implies \mathcal{S} \simeq \mathcal{Q}$, where \simeq denotes the isomorphism of two crystals as defined in Definition 2, then the crystal graph \mathcal{G} is geometrically complete. This means that if two crystal graphs $\mathcal{G}(\mathcal{S})$ and $\mathcal{G}(\mathcal{Q})$ are identical, the infinite crystal structures represented by $\mathcal{G}(\mathcal{S})$ and $\mathcal{G}(\mathcal{Q})$ are also identical. If the constructed crystal graph \mathcal{G} can distinguish any subtle structural differences between different crystal materials, it is said to be geometrically complete. According to [Widdowson and Kurlin, 2022], we present Definitions 4-6.

Definition 4: Metric. The metric d between crystal graphs \mathcal{G} satisfies all the axioms: 1) $d(\mathcal{G}(\mathcal{S}) = \mathcal{G}(\mathcal{Q})) = 0$ if and only if $\mathcal{G}(\mathcal{S}) = \mathcal{G}(\mathcal{Q})$; 2) Symmetry: $d(\mathcal{G}(\mathcal{S}), \mathcal{G}(\mathcal{Q})) = d(\mathcal{G}(\mathcal{Q}), \mathcal{G}(\mathcal{S}))$; 3) Triangle inequality: $d(\mathcal{G}(\mathcal{S}), \mathcal{G}(\mathcal{Q})) + d(\mathcal{G}(\mathcal{Q}), \mathcal{G}(\mathcal{K})) \geq d(\mathcal{G}(\mathcal{S}), \mathcal{G}(\mathcal{K}))$.

Definition 5: Lipschitz continuity of crystal graphs. If \mathcal{Q} is obtained by moving each point in the periodic crystal $\mathcal{S} \subset \mathbb{R}^n$ by no more than ϵ , and the distance of the constructed crystal graph structures satisfies $d(\mathcal{G}(\mathcal{S}), \mathcal{G}(\mathcal{K})) \leq C\epsilon$, where C is a constant, then the crys-

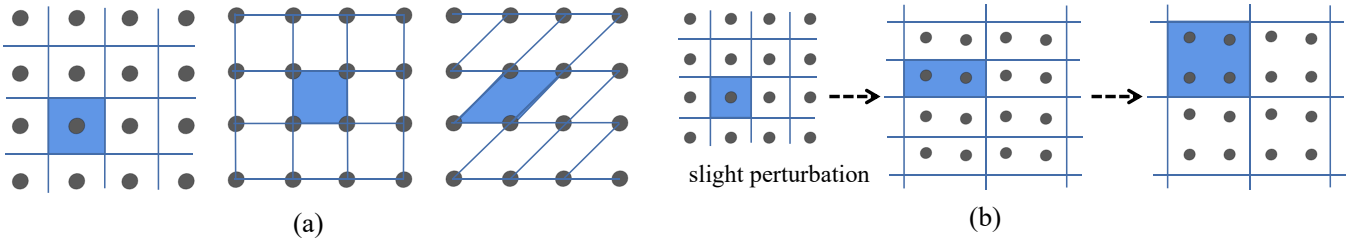


Figure 1: Illustrations of different unit cell and lattice representations of the same crystal structure. The blue area in the figure represents possible unit cell structures. Figure (a) shows several possible choices among the infinitely many unit cells for the same crystal structure in the undisturbed case. Figure (b) illustrates that for almost any perturbation, the symmetry group and any reduced unit cell (with minimal volume) will undergo discontinuous changes. This figure is derived from the original PDD Figures 1 and 2.

tal graph is continuous, and $\mathcal{Q}, \mathcal{S} \subset \mathbb{R}^n$ can be any periodic crystal structures.

Definition 6: EMD. Let $\mathcal{G}(\mathcal{S})$ and $\mathcal{G}(\mathcal{Q})$ be the crystal graph structures we construct for periodic crystals \mathcal{S} and $\mathcal{Q} \in \mathbb{R}^n$. The flow from $\mathcal{G}(\mathcal{S})$ to $\mathcal{G}(\mathcal{Q})$ is represented by an $n(\mathcal{S}) \times n(\mathcal{Q})$ matrix, where the elements $f_{ij} \in [0, 1]$ indicate the partial flow from $\mathcal{R}_i(\mathcal{S})$ to $\mathcal{R}_j(\mathcal{Q})$. The Earth Mover’s Distance (EMD) is defined as the minimum cost: $EMD(\mathcal{G}(\mathcal{S}), \mathcal{G}(\mathcal{Q})) = \sum_{i=1}^n \sum_{j=1}^n f_{ij} |R_i(\mathcal{S}) - R_j(\mathcal{Q})|$ where $f_{ij} \in [0, 1]$ satisfies the following conditions:

$$\sum_{i=0}^n f_{ij} \leq w_i(\mathcal{S}), \sum_{j=0}^n f_{ij} \leq w_j(\mathcal{Q}), \sum_{i=1}^n \sum_{j=1}^n f_{ij} = 1 \quad (1)$$

The first condition $\sum_{i=0}^n f_{ij} \leq w_i(\mathcal{S})$ means that not more than the weight $w_i(\mathcal{S})$ of the component $R_i(\mathcal{S})$ ‘flows’ into all components $R_j(\mathcal{Q})$ via ‘flows’ f_{ij} . Similarly, the second condition $\sum_{j=0}^n f_{ij} \leq w_j(\mathcal{Q})$ means that all ‘flows’ f_{ij} from $R_i(\mathcal{S})$ ‘flow’ into $R_j(\mathcal{Q})$ up to the maximum weight $w_j(\mathcal{Q})$. The last condition $\sum_{i=1}^n \sum_{j=1}^n f_{ij} = 1$ forces to ‘flow’ all rows $R_i(\mathcal{S})$ to all rows $R_j(\mathcal{Q})$.

3 Related work

Finite crystal graph representation. CGCNN [Xie and Grossman, 2018] predicts material properties by learning the connections between atoms in crystals by representing crystal structures as finite multi-edge crystal graphs. Building on the construction of multi-edge crystal graphs, MegNet [Chen *et al.*, 2019] introduced global state attributes into graph networks, while GATGNN [Louis *et al.*, 2020] utilized multiple graph attention layers (GAT) to learn the properties of local neighborhoods and employed global attention layers to weight global atomic features. ALIGNN [Choudhary and DeCost, 2021] and M3GNet [Chen and Ong, 2022] incorporated angular information into the message-passing process to generate richer and more discriminative representations. CrysMMNet [Das *et al.*, 2023] adopted a multimodal framework, integrating graph and text representations to produce joint multimodal representations of crystalline materials. CrysDiff [Song *et al.*, 2024] is a pretraining-finetuning framework based on diffusion models. However, the aforementioned methods represent crystals as finite graph structures, failing to capture the periodicity of infinite crystals effectively.

Periodic representation of crystals. Recently, Matformer [Yan *et al.*, 2022] encoded periodic patterns by adding self-

connecting edges to atoms based on lattice parameters, directly using lattice parameters to encode periodic structures under ideal conditions. PotNet [Lin *et al.*, 2023] considered the infinite summation of interatomic interactions. Crystalformer [Taniai *et al.*, 2024] performed infinite summations of interatomic potentials through infinitely connected attention while also utilizing lattice parameters. ComFormer [Yan *et al.*, 2024a] constructed cell parameters by adding self-connecting edges to atoms and their copies in three different directions to encode periodic patterns, employing equivariant vector representations and invariant geometric descriptors of Euclidean distances and angles to represent the geometric information of crystals. GMTNet [Yan *et al.*, 2024b] aims to predict the tensor properties of crystalline materials while satisfying $O(3)$ group equivariance and the symmetry of crystal space groups to ensure the accuracy and consistency of tensor predictions. However, while these methods achieve complete crystal graph representations, the crystal structures they represent rely on non-invariants or discontinuous invariants, such as lattice parameters, symmetry, and space groups, failing to address the issue of crystal data fuzziness.

Continuity and complete representations for crystals. Addressing the continuity and completeness of crystal representations is a critical issue. Recent advancements in AMD [Wang *et al.*, 2022] and PDD [Widdowson and Kurlin, 2022] have developed matrix forms that are both complete and continuous. However, in practical applications, using these matrix representations as inputs for predicting crystal properties without compromising continuity and completeness is challenging. The AMD and PDD representations are designed for stable crystal structures and do not account for atomic types. Their completeness relies on the assumption that no two crystals with identical structures differ solely by atomic type, which is only feasible for stable structures. Additionally, to achieve completeness, a sufficiently large number of neighbors k must be predetermined for any test crystal. Typically, hundreds of neighbors are required to distinguish all periodic structures in the Cambridge Structural Database. Directly modeling PDD as edge information is impractical and costly in real-world applications [Balasingham *et al.*, 2022].

4 PDDFormer

In this section, we first propose two variants of PDD, namely WPDD and UPDD, and then incorporate them into crystal

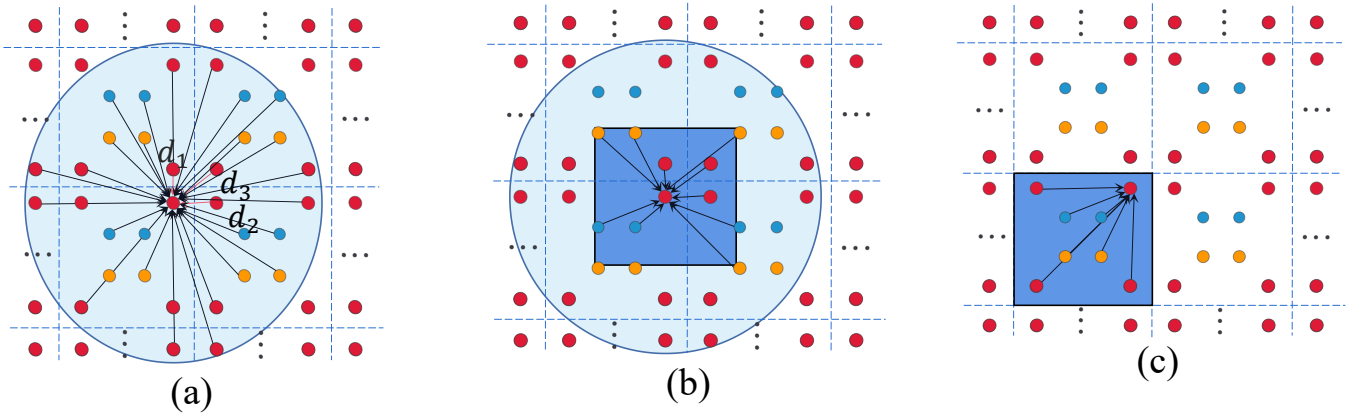


Figure 2: Schematic diagram of the selected neighbors in PDD in 2D. The edges in Figure a show the neighbor selection for atom i in WPDD, represented by the red lines d_1, d_2, d_3 . They are ordered by Euclidean distance as $d_1 < d_2 < d_3$. By comparing Figures (b) and (c), we can see that we construct the unit cell centered around each atom and select neighbors, rather than being limited to the unit cell where the atoms are located.

graph construction. We finally present the PDDformer framework.

4.1 WPDD

Since the PDD representation is designed for stable crystal structures and does not consider atomic types, it is not suitable for predicting crystal material properties. To account for the influence of atomic types, for a given crystal structure $\mathcal{S} = \mathcal{U} + \mathcal{L}$, where each atom $x_i \in \mathcal{U}$ is labeled with the atomic mass $t(x_i)$ corresponding to it, the final weight for each row is $\mathcal{W} = [w_1, \dots, w_n]^T$, where $w_i = \frac{t(x_i)}{\sum_{j=1}^n t(x_j)}$. By concatenating this with $PDD \in \mathbb{R}^{n \times k}$, an atomic-mass-weighted WPDD($\mathcal{S}; k$) $\in \mathbb{R}^{n \times (k+1)}$ is formed, represented by the following equation:

$$WPDD = (W, PDD) = \bigcup_{i=1}^n \left(\frac{t(x_i)}{\sum_{j=1}^n t(x_j)}, \bigcup_{j=1}^k \sqrt{(p_i - p_j)^2} \right) \quad (2)$$

Here, n represents the number of atoms in the unit cell, and p_i and p_j denote the spatial coordinates of an atom i and its neighbor j , respectively, and k is the number of nearest neighbors selected when constructing the PDD, sorted in ascending order of Euclidean distance as $d_{i1} \leq \dots \leq d_{ik}$, as shown in Figure ???. WPDD is equivalent to the PDD of crystal structure \mathcal{S} , except that the rows are not grouped as in the original version. This prevents the loss of atomic information when two primitive points have the same k -nearest neighbor distances but correspond to different atomic types. Therefore, $WPDD \in \mathbb{R}^{n \times (k+1)}$, where n is the number of atoms in the constructed graph.

4.2 UPDD

When ensuring the completeness of PDD, a large number of neighbors must be predefined, typically requiring information on hundreds of neighbors, and in extreme cases, the number must exceed the atom count in any unit cell within the dataset. The number of neighbors, k , is difficult to determine

across different datasets, and for unit cells with fewer atoms, which constitute a larger proportion of the dataset, an excess of neighbor information may interfere with the speed of message aggregation, leading to greater resource consumption.

To address this issue, we introduce Unit-cell PDD (UPDD). We achieve this by reconstructing the unit cell around each atom and encoding the pairwise distances between the atom and other atoms within the reconstructed unit cell. This means that when constructing PDD, we focus more on the overall structure of the atoms within the reconstructed unit cell, thereby reducing interference from excessive neighbor information. UPDD is defined by the following formula:

$$\mathcal{D}_i = \left\{ \bigcup_{j=1}^n \sqrt{(\bar{p}_i - \bar{p}_j)^2} \mid i, j \in \mathcal{Z} \right\},$$

$$(\bar{p}_i - \bar{p}_j)^2 = (\bar{x}_i - \bar{x}_j)^2 + (\bar{y}_i - \bar{y}_j)^2 + (\bar{z}_i - \bar{z}_j)^2, \quad (3)$$

$$UPDD = \left\{ \bigcup_{i=1}^n \frac{1}{\mathcal{D}_i} \mid i \in \mathcal{Z}, \mathcal{D}_i \neq 0 \right\}$$

where \mathcal{D}_i represents the union of feature vectors of distances between the atom i and other atoms within the unit cell centered on the atom i , with $\mathcal{D}_i \in \mathbb{R}^n$, and n representing the number of atoms in the unit cell. $UPDD \in \mathbb{R}^{n \times n}$ represents the union of distance features between all atoms. Since the interaction energy between an atom and its neighboring atoms is usually inversely proportional to the distance, we take the reciprocal of the distance feature after removing zeros.

As shown in Figure 2, the selection is not based on Euclidean distances, but rather on choosing atoms within the reconstructed unit cell for construction. The dimension of our UPDD is determined by the atoms in the unit cell and does not require consideration of the neighbor count, k , across different datasets, making it more generalizable. This UPDD covers unit cell structures with a larger number of atoms while also ensuring that unit cell structures with fewer atoms are not disturbed by excessive neighbor information. It also reduces resource consumption. Due to this crystal-specific treatment, the UPDD dimensions of different crystal structures may not match, so dimension alignment is required before feeding into the neural network.

4.3 Crystal graph construction

By introducing PDD, we constructed a complete and continuous multi-edge crystal graph. In the graph, each node represents an atom i and all its infinite duplicates in 3D space, with positions $\{\hat{p}_i | \hat{p}_i = p_i + k_1 l_1 + k_2 l_2 + k_3 l_3, k_1, k_2, k_3 \in \mathcal{Z}\}$, and node features x_i . An edge is established from node j to node i when the Euclidean distance $|e_{j'i}|^2$ between a duplicate of j and i satisfies $|e_{j'i}|^2 = |p_j + k'_1 l_1 + k'_2 l_2 + k'_3 l_3 - p_i|^2 \leq r$, where $r \in \mathbb{R}$ is the cutoff radius. We select the nearest t edges within the cutoff radius, each with a corresponding edge feature $|e_{j'i}|^2$. Since WPDD requires a large number of neighbors to be predefined, representing this neighbor information as edge features is neither practical nor cost-effective in real-world applications. Therefore, we retain its matrix form and incorporate it into the construction of the multi-edge crystal graph as a way to reflect the global information of the crystal structure. After passing through the Embedding Block in Section 4.6, UPDD is aligned in dimensions and transformed into matrix form data. Formally, we represent the constructed crystal graph as $\mathcal{G} = (\mathcal{X}, \mathcal{XI}, \mathcal{E}, PDD)$. Therein, $x_i \in \mathcal{X}$ is the feature vector of the atom i , $e_{ij}^h \in \mathcal{E}$ is the feature vector of the h -th edge between nodes i and j , and we denote \mathcal{XI} as the indices of the nodes i and j that form the edge. Sections 4.4 and 4.5 are our proofs of the continuity and geometric completeness of PDD crystal graphs.

4.4 Continuity of Proposed Crystal Graphs

The continuity of the constructed crystal graph $\mathcal{G}(\mathcal{S})$ under perturbations of the crystal structure \mathcal{S} will be measured using the EMD [Rubner *et al.*, 2000], which applies to crystal graphs of any size. Definition 6 applies to any crystal graph $\mathcal{G}(\mathcal{S}) = ([w_1(\mathcal{S}), R_1(\mathcal{S})], \dots, [w_1(\mathcal{S}), R_1(\mathcal{S})])$, where $[w_i(\mathcal{S}), R_i(\mathcal{S})]$ represent the information extracted based on atom i in the unit cell. $R_i(\mathcal{S}) = R_i(\mathcal{S}_{\mathcal{X}}, \mathcal{S}_{\mathcal{XI}}, \mathcal{S}_{\mathcal{E}}, \mathcal{S}_{PDD})$ includes atomic information, neighbor information used in constructing the multi-edge crystal graph, and the PDD invariants of the crystal structure \mathcal{S} , with weights $w_i \in (0, 1]$ satisfying the normalization condition $\sum_{i=1}^n w_i(\mathcal{S}) = 1$.

Subsequently, we only consider the case where the weighted vector $[w_i, R_i]$ corresponds to the i -th row of $PDD(\mathcal{S}; k)$. Here, n denotes the number of rows in $PDD(\mathcal{S}; k)$. The size of each row $R_i(\mathcal{S})$ should be independent of \mathcal{S} and depend solely on the number of neighbors k in $PDD(\mathcal{S}; k)$. For any vectors $R_i = (r_{i1}, \dots, r_{ik})$ and $R_j = (r_{j1}, \dots, r_{jk})$ of length k , we use the L_∞ -distance $|R_i - R_j|_\infty = \max_{l=0, \dots, k} |r_{il} - r_{jl}|_\infty$.

Proposition 1. The WPDD and UPDD multi-edge crystal graph is continuous.

Proof: For any $k \geq 1$, if the periodic crystal $\mathcal{S}, \mathcal{Q} \in \mathbb{R}^n$ satisfy $d_B(\mathcal{S}, \mathcal{Q}) < r(\mathcal{S})$, then we have: $EMD(\mathcal{G}(\mathcal{S}), \mathcal{G}(\mathcal{Q})) = EMD((\mathcal{S}_{\mathcal{X}}, \mathcal{S}_{\mathcal{XI}}, \mathcal{S}_{\mathcal{E}}, \mathcal{S}_{PDD}), (\mathcal{Q}_{\mathcal{X}}, \mathcal{Q}_{\mathcal{XI}}, \mathcal{Q}_{\mathcal{E}}, \mathcal{Q}_{PDD})) = EMD((\mathcal{S}_{\mathcal{X}}, \mathcal{Q}_{\mathcal{X}})) + EMD((\mathcal{S}_{\mathcal{XI}}, \mathcal{Q}_{\mathcal{XI}})) + EMD((\mathcal{S}_{\mathcal{E}}, \mathcal{Q}_{\mathcal{E}})) + EMD((\mathcal{S}_{PDD}, \mathcal{Q}_{PDD}))$. Since disturbances only change the positions of atoms and do not alter their types, therefore $EMD((\mathcal{S}_{\mathcal{X}}, \mathcal{Q}_{\mathcal{X}})) = 0$ and $EMD((\mathcal{S}_{\mathcal{XI}}, \mathcal{Q}_{\mathcal{XI}})) = 0$. So, we ob-

tain $EMD(\mathcal{G}(\mathcal{S}), \mathcal{G}(\mathcal{Q})) = EMD((\mathcal{S}_{\mathcal{E}}, \mathcal{Q}_{\mathcal{E}})) + EMD((\mathcal{S}_{PDD}, \mathcal{Q}_{PDD})) \leq 2d_B(\mathcal{S}, \mathcal{Q})$.

The bottleneck distance $d_B(\mathcal{S}, \mathcal{Q}) < r(\mathcal{S})$ is defined as: $d_B(\mathcal{S}, \mathcal{Q}) = \inf_{g: \mathcal{S} \rightarrow \mathcal{Q}} \sup_{p \in \mathcal{S}} |p - g(p)|$ and the envelope radius $r(\mathcal{S})$ is the minimum half-distance between any two points in $r(\mathcal{S})$. In other words, $r(\mathcal{S})$ is the maximum radius of non-overlapping open balls centered at all points in \mathcal{S} . This implies that any small perturbation in atomic positions under the d_B [Carstens *et al.*, 1999] will lead to minor changes in the distribution of distances between points in the EMD.

Since the EMD between the constructed crystal graphs only relates to Euclidean distance. Euclidean distance itself is continuous, Theorem 1 extends the following fact: for a unit cell structure with two atoms, when the number of neighbors $k = 1$, if we perturb at most two points by ϵ , the change in distance between the two points will be at most 2ϵ . Extending this to n atomic points with k neighbors, if we perturb at most n points by ϵ , the change in distance between n points will be at most $2nk\epsilon$. This aligns with Definition 5, hence the constructed WPDD and UPDD multi-edge crystal graph is continuous.

4.5 Geometric completeness of proposed crystal graphs

Proposition 2. The WPDD multi-edge crystal graph is geometrically complete.

Inspired by [Yan *et al.*, 2024a]. We prove this by mathematical induction. Suppose the number of atoms (nodes) in the unit cell of a crystal is n .

Base Case: When $n = 1$, the infinite crystal structure represented by the WPDD multi-edge crystal graph is unique.

Induction Hypothesis: When $n \leq m$, the infinite crystal structure is unique.

Induction Step: Let $n = m + 1$. Without loss of generality, we safely assume that among the existing mmm nodes, N_j is the set of nodes forming the local region for node j . Then, j is the index of the $(m + 1)$ -th node that is newly connected to these nodes. To prove that the infinite crystal structure remains unique, we only need to demonstrate that the relative position of node j is uniquely determined, given the WPDD multi-edge crystal graph. With this, the proposed WPDD multi-edge crystal graph can define a unique infinite crystal structure.

Here, we prove that the relative position of the newly added node j is uniquely determined by the proposed WPDD multi-edge crystal graph.

Proof: We use proof by contradiction. First, assume that there exist two distinct relative positions j and j' that have the same WPDD multi-edge crystal graph, and we show that this assumption leads to a contradiction.

Since UPDD is constructed based on the size of the unit cell, when the number of atoms in the unit cell is relatively small, it could theoretically result in different crystal structures, where all atoms have the same Euclidean distances and atom types but inconsistent atomic positions (which do not exist in the real world), sharing the same crystal graph representation. According to the WPDD multi-edge crystal graph construction process described in Section 4.3, if two distinct crystal structures have the same WPDD crystal graph, their

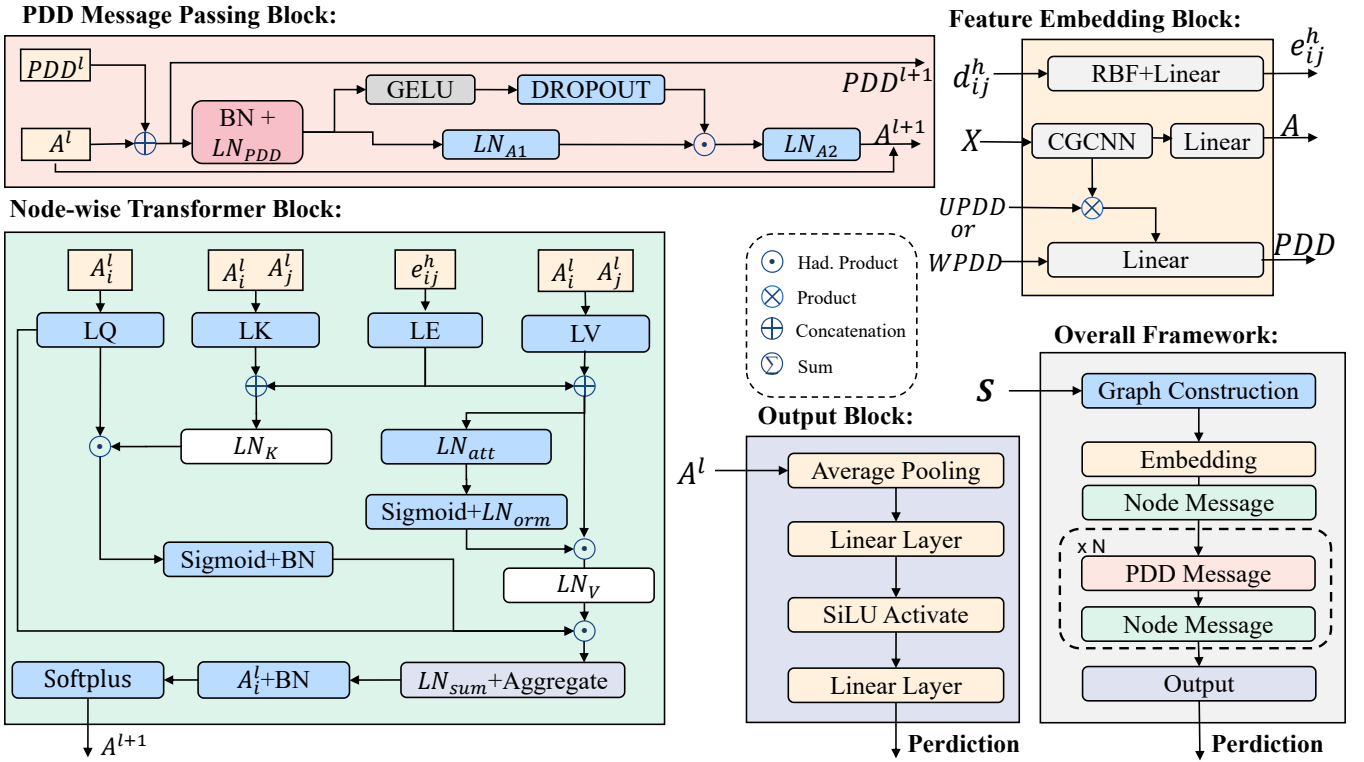


Figure 3: Illustrations of different unit cell and lattice representations of the same crystal structure. The blue area in the figure represents possible unit cell structures. Figure (a) shows several possible choices among the infinitely many unit cells for the same crystal structure in the undisturbed case. Figure (b) illustrates that for almost any perturbation, the symmetry group and any reduced unit cell (with minimal volume) will undergo discontinuous changes.

WPDD and the atomic types embedded by CGCNN must be identical. Since the WPDD crystal graph, which includes atomic information, is completely invariant, different crystal structures must have distinct WPDD crystal graphs (except for chiral crystals). This contradicts the assumption. Hence, the proof is complete. Therefore, the proposed identical crystal graph can represent only the same infinite crystal structure. Then, based on Definition 3, we complete the proof of Proposition 2.

Finally, we conclude that the UPDD crystal graph can only guarantee continuity, while the WPDD crystal graph can ensure both continuity and completeness.

4.6 Network architecture

Based on the graph in Section 4.3, we propose the information propagation scheme of PDDFormer. The information propagation scheme of PDDFormer consists of four parts: the graph embedding Block, node-wise transformer Block (inspired by [Yan *et al.*, 2024a]), PDD message passing Block, and output Block. Figure 3 illustrates the overall framework architecture of PDDFormer.

Feature embedding block. First, we introduce the construction of the graph embedding Block. We use atomic encoding from CGCNN for embedding. For the edge information e_{ij}^h , we employ radial basis functions to encode the distance between two adjacent nodes in the graph, represented by Equation 4, where γ and μ are hyperparameters.

For UPDD, due to the varying feature dimensions of UPDD for different crystals, we perform matrix multiplication on UPDD to align the structural information of different crystals, obtaining information for the PDD message passing layer. Thus, we obtain the graph embedding as:

$$A = CGCNN(\mathcal{X}), e_{ij}^h = \exp\left(-\gamma \left(\frac{\|p_i - p_j\|^2}{\mu}\right)\right), \quad (4)$$

$$PDD = UPDD \otimes A$$

where \otimes denotes the Hadamard product.

Node-wise transformer block. Building upon the constructed graph, we aggregate the node information. Let a_i^l represent the input feature vector of node i at layer l in PDDFormer. The information propagation scheme for layer l is described as follows. We use \oplus and \odot to denote concatenation and element-wise product. The message from node j to i is formed by the corresponding query q_{ij}^l , key k_{ij}^l , and value features v_{ij}^l as follows :

$$q_{ij}^l = LQ(a_i^l), k_{ij}^l = (LK(a_i^l) \oplus LK(a_j^l) \oplus LE(e_{ij}^h)),$$

$$v = (LV(a_i^l) \oplus LV(a_j^l) \oplus LE(e_{ij}^h)),$$

$$v_{ij}^l = v \odot \text{sigmoid}(LN_{orm}(LN_{att}(v))),$$

$$att^l = \frac{q_{ij}^l \odot LN_K(k_{ij}^l)}{\sqrt{d_{q_{ij}^l}}},$$

$$m_{ij}^h = q_{ij}^l + \text{sigmoid}(BN(att^l)) \odot LN_V(v_{ij}^l) \quad (5)$$

Method	Formation Energy	Bandgap(OPT)	Total Energy	Ehull	Bandgap(MBJ)
	eV/atom	eV	eV/atom	eV	eV
CFID (2018)	14	0.30	240	220	0.53
CGCNN	63	0.20	78	170	0.41
SchNet	45	0.19	47	140	0.43
MEGNET	47	0.145	58	84	0.34
GATGNN	47	0.17	56	120	0.51
ALIGNN	33.1	0.142	37	76	0.31
M3GNet	39.0	0.145	41	95	0.36
Matformer	32.5	0.137	35	64	0.30
PotNet	29.4	0.127	32	55	0.27
CrysMMNet	28.0	0.128	34	–	0.278
CrysDiff (2024)	29.0	0.131	34	62	0.287
Crystalformer	30.6	0.128	32	46	0.274
eComFormer	28.4	0.124	32	44	0.28
iComFormer	<u>27.2</u>	<u>0.122</u>	<u>28.8</u>	47	<u>0.26</u>
UPDDFormer	27.6	0.127	29.4	<u>35.6</u>	0.269
WPDDFormer	26.9	0.120	28.2	32.6	0.251

Table 1: Comparison between Zeoformer and other baselines in terms of test MAE on JARVIS dataset. The best results are shown in **bold** and the second best results are shown with underlines.

where LQ, LK, LV, and LE are the linear transformations for query, key, value, and edge features. LN_K , LN_V are the non-linear transformations for key and value, including two linear layers and an activation layer in between. LN_{update} represents the linear transformation for updating messages, and LN_{norm} denotes the layer normalization [Ba, 2016] operation. BN denotes the batch normalization layer [Ioffe, 2015], and $d_{q_{ij}^l}$ is the dimension of q_{ij}^l .

Then, we obtain the message M_i^l by aggregating the information from the neighborhood of node i over multiple edges, and A_i^{l+1} is realized as follows :

$$\begin{aligned} M_i^l &= \sum_{j \in A_i} \sum_h LN_{sum}(m_{ij}^h), \\ A_i^{l+1} &= \text{softplus}(a_i^l + BN(M_i^l)) \end{aligned} \quad (6)$$

where LN_{msg} is the linear transformation used for updating the edge messages.

PDD message passing block. A^l and PDD^l represent the atomic features and 3D periodic pattern encoding at layer l , respectively. Its message-passing mechanism is as follows:

$$\begin{aligned} \mathcal{PDD}^{l+1} &= \mathcal{PDD}^l + A^{l+1}, \\ A_1, A_2 &= LN_{PDD}(BN(\mathcal{PDD}^{l+1})), \\ A^{l+1} &= A^l + LN_{A_2}(LN_{A_1}(A_1) \odot \text{Drop}(GELU(A_2))) \end{aligned} \quad (7)$$

In this process, we update A^{l+1} using residual connections [He *et al.*, 2016].

Finally, we use average pooling to aggregate the features of all nodes in the graph, followed by a nonlinear layer, and then a linear layer to obtain the scalar output of the graph as described above. A detailed description of the PDDFormer architecture can be found in Appendix C.

5 Experiments

We conducted experiments on two material benchmark datasets, namely the Materials Project [Chen *et al.*, 2019]

and Jarvis [Choudhary *et al.*, 2020] datasets. Detailed descriptions of the datasets can be found in Appendix A. More information about the experimental settings of PDDFormer can be found in Appendix D. Baseline methods include CFID [Choudhary *et al.*, 2018], CGCNN [Xie and Grossman, 2018], SchNet [Schütt *et al.*, 2017], MEGNET [Chen *et al.*, 2019], GATGNN [Louis *et al.*, 2020], ALIGNN [Choudhary and DeCost, 2021], M3GNet [Chen and Ong, 2022], Matformer [Yan *et al.*, 2022], PotNet [Lin *et al.*, 2023], CrysMMNet [Das *et al.*, 2023], CrysDiff [Song *et al.*, 2024], Crystalformer [Taniai *et al.*, 2024], and ComFormer [Yan *et al.*, 2024a]. For all baselines on the material datasets, we report the results provided in the cited papers.

5.1 Experimental results

JARVIS. The quantitative results for JARVIS [Choudhary *et al.*, 2020] are shown in Table ???. WPDDformer achieves the best performance across all tasks. Notably, WPDDFormer and UPDDFormer outperform eComFormer by 26% and 19% respectively in the Ehull task.

The Materials Project (MP). The experimental results on MP [Chen *et al.*, 2019] are shown in Table ???. WPDDformer performs significantly better than previous works across all tasks, with a 10.8% improvement over the second-best model in the bulk moduli task. Additionally, the excellent prediction accuracy of WPDDFormer in the bulk modulus and shear modulus tasks, using only 4,664 training samples, demonstrates the expressiveness and robustness of WPDD multi-edge crystal graphs under limited training samples.

Overall, our methods are compared with 14 existing methods across the two datasets. Our WPDDFormer consistently outperforms all methods in all tasks. Additionally, WPDDFormer shows a significant improvement in prediction accuracy compared to UPDDFormer. This improvement is not only because the WPDD graph structure is complete and

Method	Formation Energy	Band Gap	Bulk Moduli	Shear Moduli
	eV/atom	eV	log(GPa)	log(GPa)
CGCNN (2018)	31	0.292	0.047	0.077
SchNet (2018)	33	0.345	0.066	0.099
MEGNET (2019)	30	0.307	0.060	0.099
GATGNN (2020)	33	0.280	0.045	0.075
ALIGNN (2021)	22	0.218	0.051	0.078
M3GNet (2022)	24	0.247	0.050	0.087
Matformer (2022)	21.0	0.211	0.043	0.073
PotNet (2023)	18.8	0.204	0.040	0.065
CrysMMNet (2023)	20.0	0.197	0.038	0.062
Crystalformer (2024)	18.6	0.198	0.0377	0.0689
eComFormer (2024)	18.16	0.202	0.0417	0.0729
iComFormer (2024)	18.26	0.193	0.0380	0.0637
UPDDFormer	18.31	0.196	0.0393	0.0686
WPDDFormer	16.61	0.189	0.0336	0.0617

Table 2: Comparison between Zeoformer and other baselines in terms of test MAE on MP dataset.

Table 3: Efficiency comparison with ConFormer on the Jarvis Formation Energy task. We show the training time per epoch, total training time, time complexity, GPU memory consumption, and total number of parameters. The experiments were conducted using a 3090 RTX 24GB GPU.

Models	Time/epoch	Total	GPU memory usage	Complexity	Model Para.
eConformer	120s	16.7h	18GB	$O(nk)$	12.4M
iConformer	129s	25.0h	12GB	$O(nk)$	5.0M
WPDDFormer	98s	10.9h	8.5GB	$O(nk)$	6.76M

Method	Num. Block	Ehull	Bulk
NO PDD Block	4,0	39.2	0.0410
without PDD	4,3	36.3	0.0400
UPDDFormer	3,2	37.4	0.0446
UPDDFormer	4,3	35.6	0.0392
WPDDFormer	3,2	34.0	0.0336
WPDDFormer	4,3	32.6	0.0341

Table 4: Num. Block represents the number of Node-wise transformer blocks and PDD message passing blocks.

continuous, while UPPD can only ensure continuity, but also because UPPD requires dimensional alignment as mentioned in 4.6, which results in some loss of the expression of global information about the unit cell.

Efficiency This experiment reports the training and inference times for WPDDFormer and ConFormer using the best model configurations. We also report the total number of parameters for each model. As shown in Table 3, all these models have a time complexity of $O(nk)$, where n represents the number of atoms in the unit cell and k represents the average number of neighbors. The data in the table is averaged over three experiments. Although WPDDFormer has a higher parameter count compared to iConFormer, its training time overhead is significantly lower than that model, and it uses less GPU memory. Its memory usage is only 70.8% of

iConFormer and 47.2% of eConFormer. This demonstrates that our WPDDFormer achieved significantly superior experimental results with lower computational cost and faster computation speed. Additional four tasks from the JARVIS dataset are documented in Appendix E.

5.2 Ablation studies

In this section, we demonstrate the impact of introducing (W/U)PDD on the representation learning of crystal materials through ablation studies. Specifically, we conducted experiments on the MP and JARVIS datasets, using testing mean absolute error (MAE) as the quantitative evaluation metric, comparing the results for **Bulk Moduli** and **Ehull** tasks, as shown in Table 4.

By comparing (W/U)PDDFormer models with different numbers of Node-wise Transformer Blocks and PDD Message Passing Blocks to models without (W/U)PDD information but retaining the *PDD* message passing blocks, we validate the importance of (W/U)PDD. The results show that compared to models without the *PDD* message passing blocks, WPDDFormer achieved improvements of 18.0% and 16.8% in the Bulk Moduli and Ehull tasks, respectively. Compared to models that retain only the *PDD* message passing blocks but lack (W/U)PDD information, we achieved improvements of 16.0% and 10.2% in these two tasks, respectively.

6 Conclusion and future work

In this study, we integrated WPDD and UPDD into the representation of crystal structures, achieving a complete and continuous construction of crystal graphs. This resolves the ambiguity in crystal graph representations for predicting the properties of crystalline materials and bridges the gap between traditional crystal descriptors and dynamic atomic behavior. Experimental results demonstrate the significant advantage of our WPDDFormer in various property prediction tasks. Ensuring the completeness and continuity of crystal graphs after incorporating angular information is a problem that will be further explored in the future.

References

- [Ahmad *et al.*, 2018] Zeeshan Ahmad, Tian Xie, Chinmay Maheshwari, Jeffrey C Grossman, and Venkatasubramanian Viswanathan. Machine learning enabled computational screening of inorganic solid electrolytes for suppression of dendrite formation in lithium metal anodes. *ACS central science*, 4(8):996–1006, 2018.
- [Ba, 2016] Jimmy Lei Ba. Layer normalization. *arXiv preprint arXiv:1607.06450*, 2016.
- [Balasingham *et al.*, 2022] Jonathan Balasingham, Viktor Zamarayev, and Vitaliy Kurlin. Compact graph representation of molecular crystals using point-wise distance distributions. *arXiv preprint arXiv:2212.11246*, 2022.
- [Balasingham *et al.*, 2024] Jonathan Balasingham, Viktor Zamarayev, and Vitaliy Kurlin. Material property prediction using graphs based on generically complete isometry invariants. *Integrating Materials and Manufacturing Innovation*, pages 1–14, 2024.
- [Bartók *et al.*, 2013] Albert P Bartók, Risi Kondor, and Gábor Csányi. On representing chemical environments. *Physical Review B—Condensed Matter and Materials Physics*, 87(18):184115, 2013.
- [Batzner *et al.*, 2022] Simon Batzner, Albert Musaelian, Lixin Sun, Mario Geiger, Jonathan P Mailoa, Mordechai Kornbluth, Nicola Molinari, Tess E Smidt, and Boris Kozinsky. E (3)-equivariant graph neural networks for data-efficient and accurate interatomic potentials. *Nature communications*, 13(1):2453, 2022.
- [Carstens *et al.*, 1999] Hans-Georg Carstens, Walter A Deuber, Wolfgang Thumser, and Elke Koppenrade. Geometrical bijections in discrete lattices. *Combinatorics, Probability and Computing*, 8(1-2):109–129, 1999.
- [Chen and Ong, 2022] Chi Chen and Shyue Ping Ong. A universal graph deep learning interatomic potential for the periodic table. *Nature Computational Science*, 2(11):718–728, 2022.
- [Chen *et al.*, 2019] Chi Chen, Weike Ye, Yunxing Zuo, Chen Zheng, and Shyue Ping Ong. Graph networks as a universal machine learning framework for molecules and crystals. *Chemistry of Materials*, 31(9):3564–3572, 2019.
- [Choudhary and DeCost, 2021] Kamal Choudhary and Brian DeCost. Atomistic line graph neural network for improved materials property predictions. *npj Computational Materials*, 7(1):185, 2021.
- [Choudhary *et al.*, 2018] Kamal Choudhary, Brian DeCost, and Francesca Tavazza. Machine learning with force-field-inspired descriptors for materials: Fast screening and mapping energy landscape. *Physical review materials*, 2(8):083801, 2018.
- [Choudhary *et al.*, 2020] Kamal Choudhary, Kevin F Garrity, Andrew CE Reid, Brian DeCost, Adam J Biacchi, Angela R Hight Walker, Zachary Trautt, Jason Hattrick-Simpers, A Gilad Kusne, Andrea Centrone, et al. The joint automated repository for various integrated simulations (jarvis) for data-driven materials design. *npj computational materials*, 6(1):173, 2020.
- [Das *et al.*, 2023] Kishalay Das, Pawan Goyal, Seung-Cheol Lee, Satadeep Bhattacharjee, and Niloy Ganguly. Crymmnet: multimodal representation for crystal property prediction. In *Uncertainty in Artificial Intelligence*, pages 507–517. PMLR, 2023.
- [Groom *et al.*, 2016] Colin R Groom, Ian J Bruno, Matthew P Lightfoot, and Suzanna C Ward. The cambridge structural database. *Structural Science*, 72(2):171–179, 2016.
- [He *et al.*, 2016] Kaiming He, Xiangyu Zhang, Shaoqing Ren, and Jian Sun. Deep residual learning for image recognition. In *Proceedings of the IEEE conference on computer vision and pattern recognition*, pages 770–778, 2016.
- [Ioffe, 2015] Sergey Ioffe. Batch normalization: Accelerating deep network training by reducing internal covariate shift. *arXiv preprint arXiv:1502.03167*, 2015.
- [Kurlin, 2024] Vitaliy Kurlin. Mathematics of 2-dimensional lattices. *Foundations of Computational Mathematics*, 24(3):805–863, 2024.
- [Lin *et al.*, 2023] Yuchao Lin, Keqiang Yan, Youzhi Luo, Yi Liu, Xiaoning Qian, and Shuiwang Ji. Efficient approximations of complete interatomic potentials for crystal property prediction. In *International Conference on Machine Learning*, pages 21260–21287. PMLR, 2023.
- [Louis *et al.*, 2020] Steph-Yves Louis, Yong Zhao, Alireza Nasiri, Xiran Wang, Yuqi Song, Fei Liu, and Jianjun Hu. Graph convolutional neural networks with global attention for improved materials property prediction. *Physical Chemistry Chemical Physics*, 22(32):18141–18148, 2020.
- [Patterson, 1944] A Lindo Patterson. Ambiguities in the x-ray analysis of crystal structures. *Physical Review*, 65(5-6):195, 1944.
- [Rubner *et al.*, 2000] Yossi Rubner, Carlo Tomasi, and Leonidas J Guibas. The earth mover’s distance as a metric for image retrieval. *International journal of computer vision*, 40:99–121, 2000.
- [Schütt *et al.*, 2017] Kristof Schütt, Pieter-Jan Kindermans, Huziel Enoc Sauceda Felix, Stefan Chmiela, Alexandre Tkatchenko, and Klaus-Robert Müller. Schnet: A

- continuous-filter convolutional neural network for modeling quantum interactions. *Advances in neural information processing systems*, 30, 2017.
- [Song *et al.*, 2024] Zixing Song, Ziqiao Meng, and Irwin King. A diffusion-based pre-training framework for crystal property prediction. In *Proceedings of the AAAI Conference on Artificial Intelligence*, volume 38, pages 8993–9001, 2024.
- [Taniai *et al.*, 2024] Tatsunori Taniai, Ryo Igarashi, Yuta Suzuki, Naoya Chiba, Kotaro Saito, Yoshitaka Ushiku, and Kanta Ono. Crystalformer: infinitely connected attention for periodic structure encoding. *arXiv preprint arXiv:2403.11686*, 2024.
- [Wang *et al.*, 2022] Rui Wang, Robin Walters, and Rose Yu. Approximately equivariant networks for imperfectly symmetric dynamics. In *International Conference on Machine Learning*, pages 23078–23091. PMLR, 2022.
- [Wassermann *et al.*, 2010] Anne Mai Wassermann, Mathias Wawer, and Jürgen Bajorath. Activity landscape representations for structure-activity relationship analysis. *Journal of medicinal chemistry*, 53(23):8209–8223, 2010.
- [Widdowson and Kurlin, 2022] Daniel Widdowson and Vitaliy Kurlin. Resolving the data ambiguity for periodic crystals. *Advances in Neural Information Processing Systems*, 35:24625–24638, 2022.
- [Widdowson *et al.*, 2022] Daniel Widdowson, Marco M Mosca, Angeles Pulido, Andrew I Cooper, and Vitaliy Kurlin. Average minimum distances of periodic point sets—foundational invariants for mapping periodic crystals. *MATCH Commun. Math. Comput. Chem*, 87(3):529–559, 2022.
- [Xie and Grossman, 2018] Tian Xie and Jeffrey C Grossman. Crystal graph convolutional neural networks for an accurate and interpretable prediction of material properties. *Physical review letters*, 120(14):145301, 2018.
- [Yan *et al.*, 2022] Keqiang Yan, Yi Liu, Yuchao Lin, and Shuiwang Ji. Periodic graph transformers for crystal material property prediction. *Advances in Neural Information Processing Systems*, 35:15066–15080, 2022.
- [Yan *et al.*, 2024a] Keqiang Yan, Cong Fu, Xiaofeng Qian, Xiaoning Qian, and Shuiwang Ji. Complete and efficient graph transformers for crystal material property prediction. *arXiv preprint arXiv:2403.11857*, 2024.
- [Yan *et al.*, 2024b] Keqiang Yan, Alexandra Saxton, Xiaofeng Qian, Xiaoning Qian, and Shuiwang Ji. A space group symmetry informed network for $o(3)$ equivariant crystal tensor prediction. *arXiv preprint arXiv:2406.12888*, 2024.
- [Zwart *et al.*, 2008] Peter H Zwart, Ralf W Grosse-Kunstleve, Andrey A Lebedev, Garib N Murshudov, and Paul D Adams. Surprises and pitfalls arising from (pseudo) symmetry. *Acta Crystallographica Section D: Biological Crystallography*, 64(1):99–107, 2008.